Prabha Materials Science Letters
Vol. 1, No. 1, 21-29, 2022
https://doi.org/10.33889/PMSL.2022.1.1.004

X-ray Absorption Spectroscopy for Estimation of Oxidation State, Chemical Fraction and Local Atomic Structure of Materials

Jitendra Pal Singh
Department of Physics,
Manav Rachna University, Faridabad-121004, Haryana, India.
Corresponding author: jitendra_singh2029@rediffmail.com

Subhajit Nandy
Advanced Analysis Center,
Korea Institute of Science and Technology,
Seoul-02792, Republic of Korea.

Keun Hwa Chae
Advanced Analysis Center,
Korea Institute of Science and Technology,
Seoul-02792, Republic of Korea.

Sangsul Lee
Pohang Accelerator Laboratory,
Pohang University of Science and Technology,
Pohang-37673, Republic of Korea.

(Received on June 17, 2022 ; Accepted on July 21, 2022)

Abstract
This work discussed the role of X-ray absorption spectroscopy (XAS) in determining the oxidation state, chemical fraction, and local atomic structure of the materials. These aspects of XAS were discussed by taking $LiNiO_2$ and Mn_3O_4 as prototype materials. The oxidation state of metal ions in these oxides was estimated with the help of XAS spectra of the reference oxides such as NiO (in the case of $LiNiO_2$), MnO, Mn_2O_3, and MnO_2 (in the case of Mn_3O_4). Analysis of the oxidation state was performed from the main absorption edge which was estimated from half of the step height. This showed that the Ni K-edge absorption edge of $LiNiO_2$ is slightly above that of NiO. In the case of Mn ions, the main absorption edges show a linear variation with the oxidation states. This estimates the presence of a mixed oxidation state (2.6+) of Mn ions in Mn_3O_4. Linear combination fitting results exhibit that almost 35% of ions are in a 2+ oxidation state. The remaining ions are in a 3+ oxidation state. Thus, XAS can determine the fractions of each oxidation state of a particular ion in a given material. Quantitative information on coordination number and bond distance of nearest neighbor for a given element of a material is another important use of this technique.

Keywords- X-ray absorption spectroscopy; Oxidation state; Chemical fraction; Local atomic structure.

1. Introduction

X-ray absorption spectroscopy (XAS) is based on the probing orbitals of atoms by varying X-ray energy (Yano & Yachandra, 2009; Gaur et al., 2013). Depending on the availability of X-ray energy, it can probe atoms from Hydrogen to Uranium. As the main requirement of XAS is a variation of X-ray energy, hence, X-ray sources that can provide tunable X-rays are essential. This can be achieved by using a synchrotron source (Bilderback et al., 2005). Thus, numerous storage rings are developed across the world to produce synchrotron X-rays (Bharti and Goyal, 2019).

By its nature of probing atoms/ions of materials, XAS is widely used to investigate phenomena that have important applications in physics (Oyanagi, 2007), chemistry (Penner-Hahn, 1999), materials science (Frahm et al., 2009, Kerr et al., 2022), biomedical (Ortega et al., 2012, Buzanich, 2022), environment (Ginder-Vogel et al., 2009), agriculture (Fendorf, 1994) and other important disciplines (Carrington et al., 2002; Iglesias-Juez et al., 2022). The X-ray absorption near edge structure (XANES) region of the XAS technique gives information of oxidation state in materials (Hall et al., 2007). There are reports, which are based on the determination of the metallic oxidation state in tissues (Kwiatek et al., 2001), artificially created enzyme (Najafpour et al., 2017), and establishment of metallic form of Au (Dwivedi et al., 2017a) from the analysis of XANES region. The broad region of XAS, which is also known as extended X-ray absorption fine structure (EXAFS) depicts information on the atomic environment of metallic ions in waste **(**Dwivedi et al., 2017b), coordination of metallic ions in oxides (Boubnov et al., 2015; Kaur et al., 2020), and bond-distance in various materials systems (Gagné & Hawthorne, 2020; Singh et al., 2018a Singh et al., 2021). The establishment of vacancies in materials (Zhu et al., 2020; Wang & Wang, 2021) and determining their nature is another important application of this technique (Sung et al., 2017; Singh et al., 2019; Soni et al., 2020;). Thus, the objective of this work is to highlight the importance of the XAS in determining material characteristics. Materials such as $LiNiO_2$ and Mn_3O_4 are taken to achieve this objective.

2. Experimental Details

The XAS measurements on Ni and Mn K-edges of $LiNiO_2$ and Mn_3O_4 respectively were performed at the 1D KIST beamline of Pohang Accelerator Laboratory (PAL), Pohang, South Korea (Gianolio, 2016). This beamline operates in top-up mode with the energy of 3 GeV and a beam current of 300 mA. Si (111) monochromators are used to select energy from a broad energy range of 4-20 keV with an energy resolution of 10^{-4}. Materials for these measurements were procured from Alfa Aesar. Measured XAS spectra are normalized and converted to k-space by using ATHENA while the k^2-weighted EXAFS data is simulated using ARTEMIS (Ravel & Newville, 2005; Husain et al., 2021).

3. Results and Discussion

In this section, results obtained from the XAS study of $LiNiO_2$ and Mn_3O_4 are discussed.

3.1 $LiNiO_2$

$LiNiO_2$ is one of the important materials that are well known for their applications in rechargeable batteries as cathodes (Yamada et al., 1995, Kurzhals et al., 2021). $LiNiO_2$ has a layered structure formed by NiO_2 stacks with intercalating Li layers. Ni ions are arranged in the form of octahedral coordination with oxygen ions in the material (Chung et. al. 2005). To throw light on the Ni oxidation state in this material, XAS spectra of Ni metal (Ni oxidation state = 0) and NiO (Ni oxidation state = 2+) are also measured along with this oxide. XAS signals obtained from the Ni K-edge of these materials are shown in Figure 1a. These spectra depict a clear difference in the structures (rectangular region) which are due to the different coordination environment of Ni ions with the nearest neighbor (Guda et al., 2021). The oxidation state of Ni ions in $LiNiO_2$ materials is probed by comparing the XANES spectrum to that of Ni and NiO (Figure 1b). The main edges were estimated from half of the step height. Arrow in the Figure 1b depicts step height. The estimated values of main edges are 8332.4, 8340.2, and 8340.7 eV for Ni, NiO, and $LiNiO_2$ materials. The main edge for $LiNiO_2$ is higher than that of NiO. This may be due to the presence of Ni ions in 3+ oxidation state as predicted by the ionic model (Li et al., 2021; Genreith-Schriever et al., 2022). k^2-weighted EXAFS spectra of these materials show a clear difference in the oscillation patterns which are due to the different kinds of environments of Ni ions in each material (Figure 1c). This behavior is also reflected in the rectangular region of Figure 1a. Non-phase corrected Fourier transform of simulated EXAFS spectra are shown in Figure 1d for Ni, NiO, and $LiNiO_2$ (Pugliese

et al., 2022). A quick first shell approach was used to simulate the spectrum by taking Ni-O at 2.50 Å in the case of Ni. On the other hand, two shells, Ni-O and Ni-Ni at 2.00 and 2.85 Å are considered for the case of oxides. Simulated parameters obtained by fitting the spectra are collated in Table 1.

Table 1. Co-ordination number (N), Bond-distance (R), Debye-Waller factor (σ^2), and inner potential shift (ϵ_0) estimated from Ni K-edge spectra of Ni, NiO, and $LiNiO_2$. R-factor represents the goodness of fit.

Materials	Shell	N	R (Å)	σ^2 (Å^2)	ϵ_0 (eV)	R-Factor
Ni	Ni-Ni	12.0	2.48±0.01	0.006±0.001	6.5	0.002
NiO	Ni-O	6.3±0.8	2.06±0.01	0.005	-5.5	0.02
	Ni-Ni	12.4±0.8	2.94±0.02	0.005	-5.5	
	Ni-O	5.9±0.6	2.01±0.02	0.018	-0.6	0.01
$LiNiO_2$	Ni-Ni	6.6±1.1	2.92±0.01	0.006±0.001	-0.6	

In the case of Ni metal, Ni ions are surrounded by 12 Ni ions, however, Ni ions in NiO have a different atomic environment as it is surrounded by 6 oxygen and 12 Ni ions. It can be seen clearly that $LiNiO_2$ has a different atomic environment as it is surrounded by 6 oxygen and 6 Ni ions. This has been reflected in the quantitative analysis in Table 1.

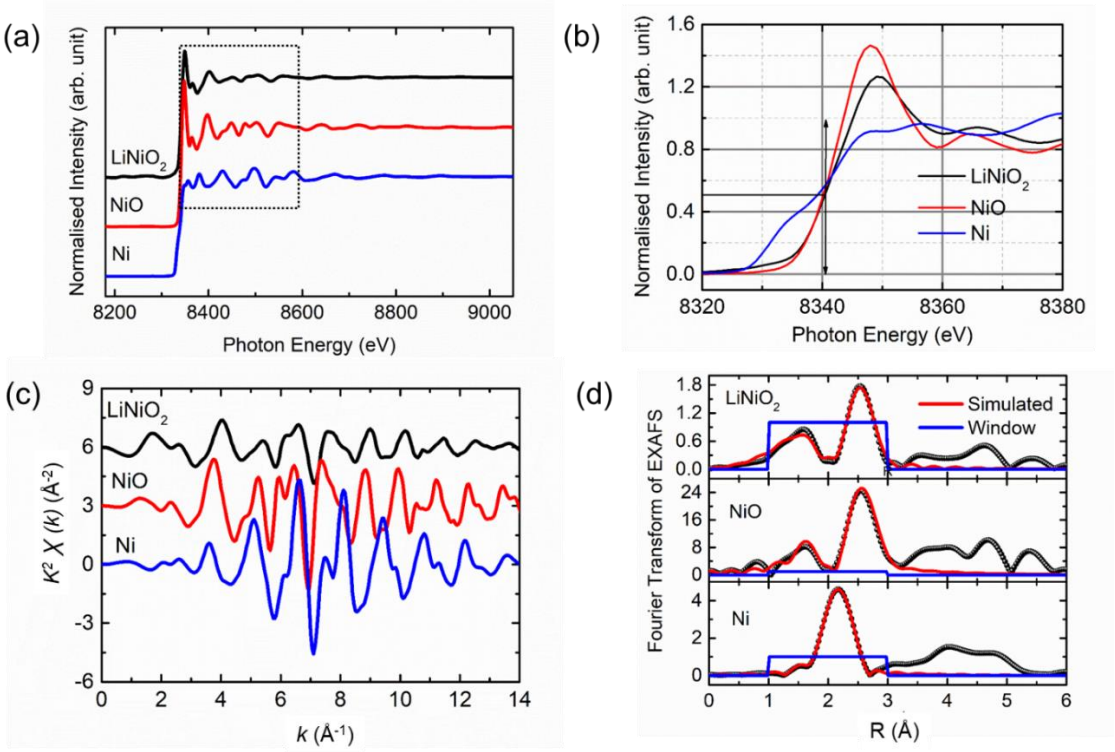

Figure 1. Ni K-edge (a) XAS spectra, (b) XANES spectra, (c) k^2-weighted EXAFS spectra, and (d) the Fourier transform of EXAFS signals for Ni, NiO, and $LiNiO_2$. In (d), solid circular symbols, curve lines, and straight-line represent the experimental data, simulated curves, and the fitted window respectively.

3.2 Mn_3O_4

Mn_3O_4 is an important material, which finds applications in numerous fields (Chen et al., 2018; Han et al.,

2020; Stoševski et al., 2021). This material exhibits a tetragonal spinel structure (Chang et al., 2004, Hirai et al., 2015). The structure may be tuned to orthorhombic depending upon the method of synthesis (Hu et al., 2017). Hence, Mn K-edge XAS measurements were performed on this material along with reference materials such as Mn (oxidation state = 0), MnO (oxidation state = 2+), Mn_2O_3 (oxidation state = 3+), and MnO_2 (oxidation state = 4+). The Mn K-edge XAS measurements of these materials are shown in Figure 2a. Analogues to Figure 1a, structures in the rectangular region are different, indicating the differences in the coordination environment of each oxide (Figure 2a). The normalized XANES spectra of these materials are shown in Figure 2b. Estimated values corresponding to the main edge as a function of the oxidation state are shown in Figure 2c. The variation is almost linear and follows the following empirical relation in the case of the Mn oxidation state.

$$E_o = (2.8 \pm 0.1) * x + (6538.7 \pm 0.4) \quad (1)$$

where E_o is the main absorption edge of the element and x is the oxidation state of the ion.

Mn K-edge for Mn_3O_4 is 6545.4 eV. Using Equation 1, the oxidation state of Mn ions in Mn_3O_4 is estimated to be 2.6+. To estimate the fraction of each oxidation state, linear combination fitting (Dwivedi, et al., 2017c; Singh et al., 2018b) on the XANES spectra of Mn_3O_4 was applied by taking spectra of MnO and Mn_2O_3 as references. This estimates that fractions of 2+ and 3+ oxidation states are 35 and 65 % respectively.

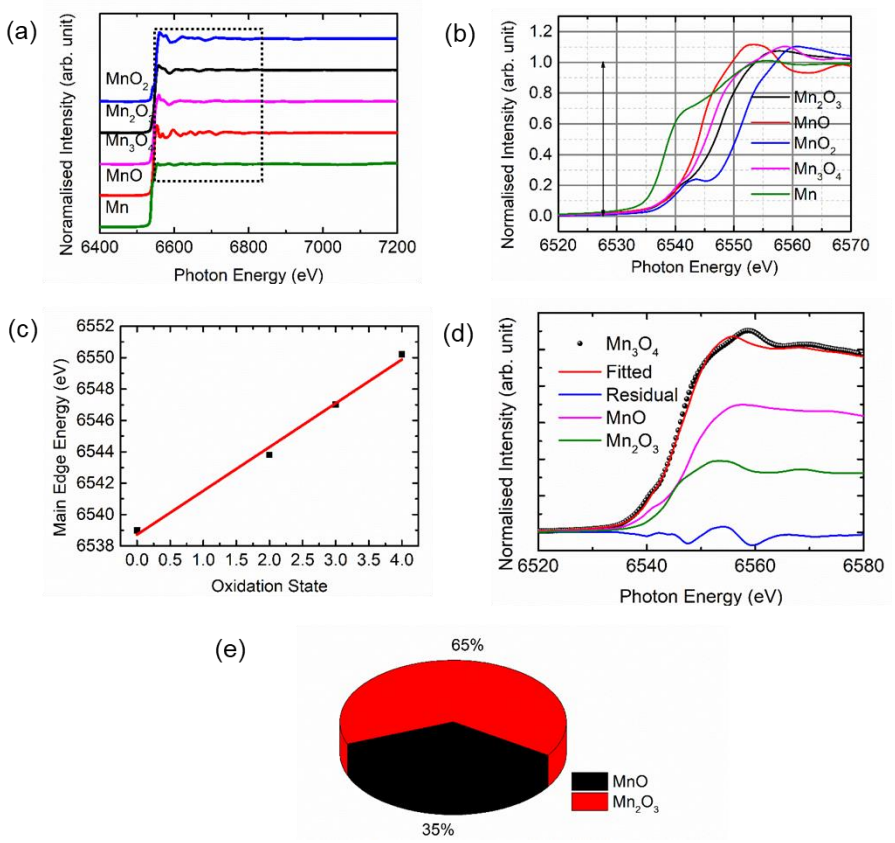

Figure 2. Mn K-edge (a) XAS and (b) XANES spectra of Mn, MnO, Mn_3O_4, Mn_2O_3, and MnO_2. (c) Variation of main-edge energies with oxidation states of Mn and (d) linear combination fitting of Mn_3O_4 for MnO and Mn_2O_3 as references (e) pi-diagram showing the fractions of 2+ (MnO) and 3+ (Mn_2O_3) in Mn_3O_4.

To investigate the local atomic structure, the EXAFS spectrum of Mn_3O_4 is simulated. The simulated spectrum is shown in Figure 3. Simulated parameters are collated in Table 2. Co-ordination numbers and bond-distances are in agreement with a previously published report by Fritsch et al. (1998).

Table 2. Co-ordination number (N), bond-distance (R), Debye-Waller factor (σ^2), and inner potential shift (ϵ_o) estimated from Mn K-edge spectra of Mn_3O_4. R-factor represents the goodness of fit.

Shell	N	R (Å)	σ^2 (Å^2)	ϵ_o (eV)	R-Factor
Mn-O	4.5	1.93	0.003	2.04	0.09
Mn-O	0.7	2.41	-0.012	2.04	

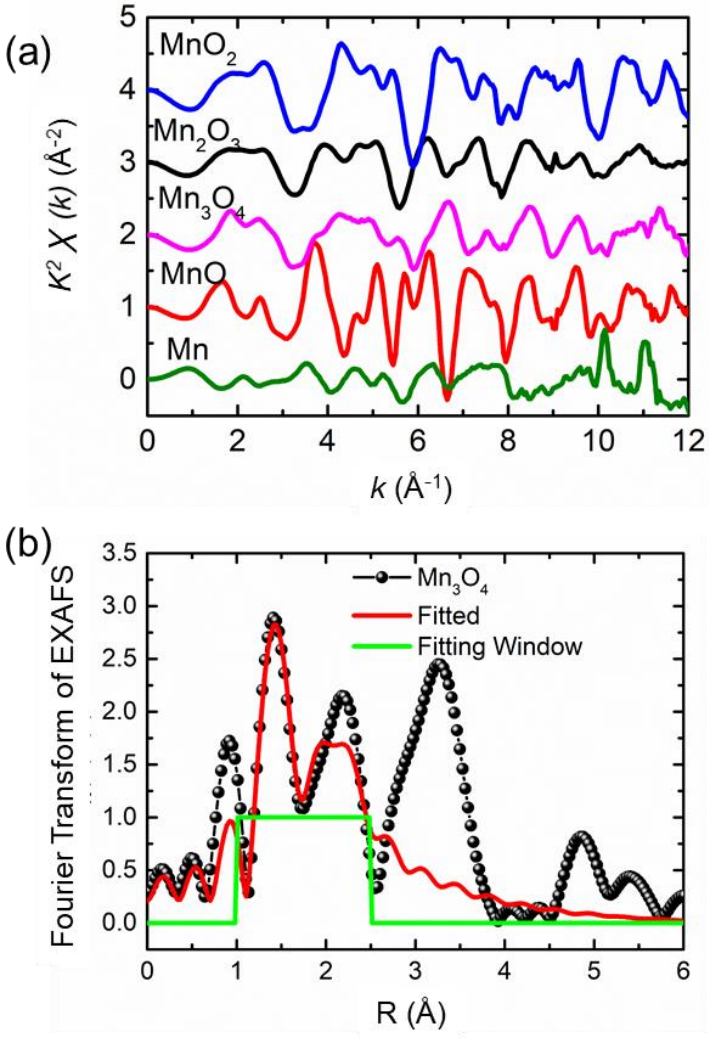

Figure 3. Mn K-edge (a) k^2-weighted χ(k) *vs* k spectra of Mn, MnO, Mn_3O_4, Mn_2O_3, and MnO_2 and (b) simulated non-phase corrected Fourier transform of EXAFS spectra of Mn_3O_4.

4. Conclusion

Thus, this work demonstrates the use of X-ray absorption spectroscopy in determining the oxidation state, fraction of each oxidation state, coordination number, and bond-distance in different oxide materials. In the case of $LiNiO_2$, the value of main edge is higher than that of NiO showing the oxidation state of Ni higher than 2+. Mn K-edge XAS study shows that the main edge varies almost linearly with Mn oxidation state. In the case of Mn_3O_4, Mn oxidation is almost 2.6+. Further, linear combination fitting shows that the atomic fraction of 2+ oxidation state is almost 35%. Simulation of EXAFS spectra show that Ni ions are surrounded by 6 equidistant oxygen ions in $LiNiO_2$, however, the case is different for Mn_3O_4. Though Mn ions are surrounded by 6 oxygen ions but they are not placed at the same distance.

Conflict of Interest

The authors confirm that there is no conflict of interest to declare for this publication.

Acknowledgments

This research did not receive any specific grant from funding agencies in the public, commercial, or not-for-profit sectors.

References

Bharti, A., & Goyal, N. (2019). Fundamental of synchrotron radiations. In: Joseph, D. (ed) *Synchrotron Radiation-Useful and Interesting Applications*. IntechOpen. London. https://doi.org/10.5772/intechopen.82202.

Bilderback, D.H., Elleaume, P., & Weckert, E. (2005). Review of third and next generation synchrotron light sources. *Journal of Physics B: Atomic, Molecular and Optical Physics*, *38*(9), S773.

Boubnov, A., Lichtenberg, H., Mangold, S., & Grunwaldt, J.D. (2015). Identification of the iron oxidation state and coordination geometry in iron oxide-and zeolite-based catalysts using pre-edge XAS analysis. *Journal of Synchrotron Radiation*, *22*(2), 410-426.

Buzanich, A.G. (2022). Recent developments of X-ray absorption spectroscopy as analytical tool for biological and biomedical applications. *X-Ray Spectrometry*, *51*(3), 294-303.

Carrington, P.E., Al-Mjeni, F., Zoroddu, M.A., Costa, M., & Maroney, M.J. (2002). Use of XAS for the elucidation of metal structure and function: applications to nickel biochemistry, molecular toxicology, and carcinogenesis. *Environmental Health Perspectives*, *110*(5), 705-708.

Chang, Y.Q., Xu, X.Y., Luo, X.H., Chen, C.P., & Yu, D.P. (2004). Synthesis and characterization of Mn_3O_4 nanoparticles. *Journal of Crystal Growth*, *264*(1-3), 232-236.

Chen, D., Yang, B., Jiang, Y., & Zhang, Y.Z. (2018). Synthesis of Mn_3O_4 nanoparticles for catalytic application via ultrasound-assisted ball milling. *Chemistry Select*, *3*(14), 3904-3908.

Chung, J.H., Proffen, T., Shamoto, S., Ghorayeb, A.M., Croguennec, L., Tian, W., Sales, B.C., Jin, R., Mandrus, D., & Egami, T. (2005). Local structure of Li Ni O_2 studied by neutron diffraction. *Physical Review B*, *71*(6), 064410.

Dwivedi, A.D., Permana, R., Singh, J.P., Yoon, H., Chae, K.H., Chang, Y.S., & Hwang, D.S. (2017a). Tunichrome-inspired gold-enrichment dispersion matrix and its application in water treatment: a proof-of-concept investigation. *ACS Applied Materials & Interfaces*, *9*(23), 19815-19824.

Dwivedi, A.D., Permana, R., Singh, J.P., Yoon, H., Chae, K.H., Chang, Y.S., & Hwang, D.S. (2017c). Tunichrome mimetic matrix, its perspective in abatement for carcinogenic hexavalent chromium and specific coordination behavior. *Chemical Engineering Journal*, *328*, 629-638.

Dwivedi, A.D., Sanandiya, N.D., Singh, J.P., Husnain, S.M., Chae, K.H., Hwang, D.S., & Chang, Y.S. (2017b). Tuning and characterizing nanocellulose interface for enhanced removal of dual-sorbate (AsV and CrVI) from water matrices. *ACS Sustainable Chemistry & Engineering*, *5*(1), 518-528.

Fendorf, S.E., Sparks, D.L., Lamble, G.M., & Kelley, M.J. (1994). Applications of X-ray absorption fine structure spectroscopy to soils. *Soil Science Society of America Journal*, *58*(6), 1583-1595. https://doi.org/10.2136/sssaj1994.03615995005800060001x.

Frahm, R., Wagner, R., Herdt, A., & Lützenkirchen-Hecht, D. (2009, November). XAS at the materials science X-ray beamline BL8 at the DELTA storage ring. In *Journal of Physics: Conference Series* (Vol. 190, No. 1, p. 012040). IOP Publishing. Italy.

Fritsch, S., Sarrias, J., Rousset, A., & Kulkarni, G.U. (1998). Low-temperature oxidation of Mn_3O_4 hausmannite. *Materials Research Bulletin*, *33*(8), 1185-1194.

Gagné, O.C., & Hawthorne, F.C. (2020). Bond-length distributions for ions bonded to oxygen: Results for the transition metals and quantification of the factors underlying bond-length variation in inorganic solids. *IUCrJ*, *7*(4), 581-629.

Gaur, A., Shrivastava, B.D., & Nigam, H.L. (2013). X-ray absorption fine structure (XAFS) spectroscopy–a review. *Proceedings of the Indian National Science Academy*, *79*(Part B), 921-966.

Genreith-Schriever, A.R., Banerjee, H., Grey, C.P., & Morris, A.J. (2022). Ni-O-redox, oxygen loss and singlet oxygen formation in $LiNiO_2$ cathodes for Li-ion batteries. *arXiv preprint arXiv:2205.10462*. https://doi.org/10.48550/arXiv.2205.10462.

Gianolio, D. (2016). How to start an XAS experiment. *X-Ray Absorption and X-Ray Emission Spectroscopy: Theory and Applications*, *1*.

Ginder-Vogel, M., Landrot, G., Fischel, J.S., & Sparks, D.L. (2009). Quantification of rapid environmental redox processes with quick-scanning x-ray absorption spectroscopy (Q-XAS). *Proceedings of the National Academy of Sciences*, *106*(38), 16124-16128.

Guda, A.A., Guda, S.A., Martini, A., Kravtsova, A.N., Algasov, A., Bugaev, A., Kubrin, S.P., Guda, L.V., Šot, P., van Bokhoven, J.A., Copéret, C., & Soldatov, A.V. (2021). Understanding X-ray absorption spectra by means of descriptors and machine learning algorithms. *NPJ Computational Materials*, *7*(1), 1-13.

Hall, M.D., Underwood, C.K., Failes, T.W., Foran, G.J., & Hambley, T.W. (2007). Using XANES to monitor the oxidation state of cobalt complexes. *Australian Journal of Chemistry*, *60*(3), 180-183.

Han, R., Zhang, Y., & Xie, Y. (2020). Application of Mn_3O_4 nanowires in the dye waste water treatment at room temperature. *Separation and Purification Technology*, *234*(1), 116119.

Hirai, S., Goto, Y., Sakai, Y., Wakatsuki, A., Kamihara, Y., & Matoba, M. (2015). The electronic structure of structurally strained Mn_3O_4 postspinel and the relationship with Mn3O4 spinel. *Journal of the Physical Society of Japan*, *84*(11), 114702.

Hu, Y., Zhang, Y., Yuan, D., Li, X., Cai, Y., & Wang, J. (2017). Controllable structure transitions of Mn_3O_4 nanomaterials and their effects on electrochemical properties. *Nanoscale Horizons*, *2*(6), 326-332.

Husain, H., Sulthonul, M., Hariyanto, B., Cholsuk, C., & Pratapa, S. (2021). Technical aspects of EXAFS data analysis using Artemis software. *Materials Today: Proceedings*, *44*(3), 3296-3300.

Iglesias-Juez, A., Chiarello, G.L., Patience, G.S., & Guerrero-Pérez, M.O. (2022). Experimental methods in chemical engineering: X-ray absorption spectroscopy—XAS, XANES, EXAFS. *The Canadian Journal of Chemical Engineering*, *100*(1), 3-22.

Kaur, B., Bhardwaj, R., Singh, J.P., Asokan, K., Chae, K.H., Goyal, N., & Gautam, S. (2020, May). Valence state and co-ordination of implanted ions in MgO. In *AIP Conference Proceedings* (Vol. 2220, No. 1, p. 090003). AIP Publishing LLC. https://doi.org/10.1063/5.0001400.

Kerr, B.V., King, H.J., Garibello, C.F., Dissanayake, P.R., Simonov, A.N., Johannessen, B., & Hocking, R.K. (2022). Characterization of energy materials with X-ray absorption spectroscopy─ advantages, challenges, and opportunities. *Energy & Fuels*, *36*(5), 2369-2389.

Kurzhals, P., Riewald, F., Bianchini, M., Sommer, H., Gasteiger, H.A., & Janek, J. (2021). The $LiNiO_2$ cathode active material: a comprehensive study of calcination conditions and their correlation with physicochemical properties. part i. structural chemistry. *Journal of The Electrochemical Society*, *168*(11), 110518.

Kwiatek, W.M., Gałka, M., Hanson, A.L., Paluszkiewicz, C., & Cichocki, T. (2001). XANES as a tool for iron oxidation state determination in tissues. *Journal of Alloys and Compounds*, *328*(1-2), 276-282.

Li, H., Hua, W., Liu-Théato, X., Fu, Q., Desmau, M., Missyul, A., Knapp, M., Ehrenberg, H., & Indris, S. (2021). New insights into lithium hopping and ordering in $LiNiO_2$ cathodes during Li (De) intercalation. *Chemistry of Materials*, *33*(24), 9546-9559.

Najafpour, M.M., Madadkhani, S., Akbarian, S., Hołyńska, M., Kompany-Zareh, M., Tomo, T., Singh, J.P., Chae, K.H., & Allakhverdiev, S.I. (2017). A new strategy to make an artificial enzyme: photosystem II around nanosized manganese oxide. *Catalysis Science & Technology*, *7*(19), 4451-4461.

Ortega, R., Carmona, A., Llorens, I., & Solari, P.L. (2012). X-ray absorption spectroscopy of biological samples. A tutorial. *Journal of Analytical Atomic Spectrometry*, *27*(12), 2054-2065.

Oyanagi, H. (2007, March). Unconventional XAS applications in physical science using pixel array X-ray detector. In *AIP Conference Proceedings* (Vol. 902, No. 1, pp. 99-102). American Institute of Physics. https://doi.org/10.1063/1.2723632.

Penner-Hahn, J.E. (1999). X-ray absorption spectroscopy in coordination chemistry. *Coordination Chemistry Reviews*, *190*, 1101-1123.

Pugliese, G.M., Capone, F.G., Tortora, L., Stramaglia, F., Simonelli, L., Marini, C., Kondoh, Y., Kajita, T., Katsufuji, T., Mizokawa, T., & Saini, N.L. (2022). The local structure and metal-insulator transition in a Ba_3Nb_5− xTi_xO_{15} system. *Materials*, *15*(13), 4402. https://doi.org/10.3390/ma15134402.

Ravel, B., & Newville, M. (2005). ATHENA, ARTEMIS, HEPHAESTUS: data analysis for X-ray absorption spectroscopy using IFEFFIT. *Journal of Synchrotron Radiation*, *12*(4), 537-541.

Singh, J.P., Kaur, B., Sharma, A., Kim, S.H., Gautam, S., Srivastava, R.C., Goyal, N., Lim, W.C., Lin, H-J, Chen, J.M., Asokan, K., Kanjilal, D., Won, S.O., Lee, I.-J., & Chae, K.H. (2018b). Mechanistic insights into the interaction between energetic oxygen ions and nanosized $ZnFe_2O_4$: XAS-XMCD investigations. *Physical Chemistry Chemical Physics*, *20*(17), 12084-12096.

Singh, J.P., Lim, W.C., & Chae, K.H. (2019). An interplay among the Mg^{2+} ion coordination, structural order, oxygen vacancies and magnetism of MgO thin films. *Journal of Alloys and Compounds*, *806*, 1348-1356.

Singh, J.P., Lim, W.C., Won, S.O., Song, J., & Chae, K.H. (2018a). Synthesis and characterization of some alkaline-earth-oxide nanoparticles. *Journal of the Korean Physical Society*, *72*(8), 890-899.

Singh, V., Paidi, A.K., Shim, C.H., Kim, S.H., Won, S.O., Singh, J.P., Lee, S., & Chae, K.H. (2021). Calcite nanocrystals investigated using X-ray absorption spectroscopy. *Crystals*, *11*(5), 490.

Soni, S., Dave, M., Dalela, B., Alvi, P.A., Kumar, S., Sharma, S.S., Phase, D.M., Gupta, M., & Dalela, S. (2020). Effect of defects and oxygen vacancies on the RTFM properties of pure and Gd-doped CeO_2 nanomaterials through soft XAS. *Applied Physics A*, *126*(8), 1-11.

Stoševski, I., Bonakdarpour, A., Fang, B., Voon, S.T., & Wilkinson, D.P. (2021). Hausmannite Mn_3O_4 as a positive active electrode material for rechargeable aqueous Mn-oxide/Zn batteries. *International Journal of Energy Research*, *45*(1), 220-230.

Sung, N.E., Lee, H.K., Chae, K.H., Singh, J.P., & Lee, I.J. (2017). Correlation of oxygen vacancies to various properties of amorphous zinc tin oxide films. *Journal of Applied Physics*, *122*(8), 085304.

Wang, Z., & Wang, L. (2021). Role of oxygen vacancy in metal oxide based photoelectrochemical water splitting. *EcoMat*, *3*(1), e12075.

Yamada, S., Fujiwara, M., & Kanda, M. (1995). Synthesis and properties of $LiNiO_2$ as cathode material for secondary batteries. *Journal of Power Sources*, *54*(2), 209-213.

Yano, J., & Yachandra, V.K. (2009). X-ray absorption spectroscopy. *Photosynthesis Research*, *102*(2), 241-254.

Zhu, K., Shi, F., Zhu, X., & Yang, W. (2020). The roles of oxygen vacancies in electrocatalytic oxygen evolution reaction. *Nano Energy*, *73*, 104761.

Original content of this work is copyright © Prabha Materials Science Letters. Uses under the Creative Commons Attribution 4.0 International (CC BY 4.0) license at https://creativecommons.org/licenses/by/4.0/